Multi-particle production

The process $p_a + p_b \to p_1 + \ldots + p_n$ depends on $3n–4$ essential variables (see chapter 1) and can be described in numerous ways. Let's here concentrate on 2 methods that with some modifictions are the descriptions used in modern HEP event generators. It is possible to visualize a multi-particle reaction as taking place via resonance formation & decay. In the intermediate state, there are unstable particles, which successively decays to others & eventually form the final state particles. The alternative is to use a multi-peripheral mechanism, implying the dominance of a diagram of the type exhibited in the 2nd figure. Regardless of the actual validity of such dynamical ideas, we shall show that kinematically an n–particle final state can always be subdivided into simpler processes. This means that the phase space integral R_n can be recursively expressed in terms of R_l's, where $l < n$. The 2 methods needs to be seperated since in the 1st one, all the intermediate systems occuring have timelike total four-momenta & hence one can go to their rest frames and parametrize vectors by spherical angles.

(E.Byckling & K.Kajantie)

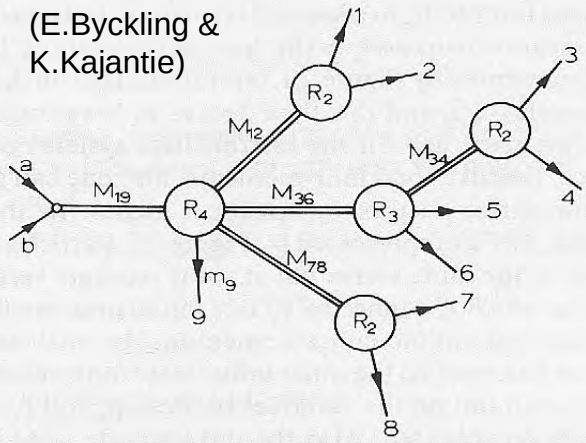

Figure VI.2.1 Example of cascade decay. Double lines denote systems of particles. Total energy is fixed. In this figure $M_{19}^2 = (p_1 + p_2 + \ldots + p_9)^2$, etc.

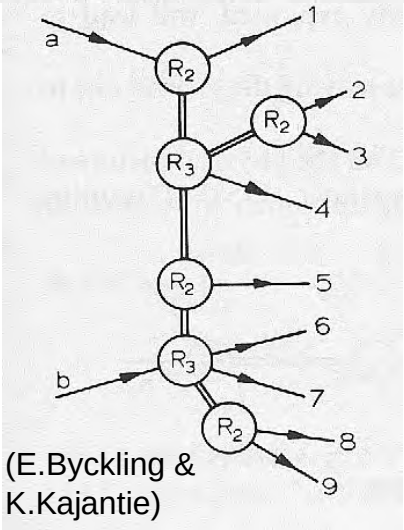

(E.Byckling & K.Kajantie)

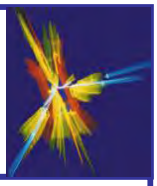

In the 2nd case, particles a & b do not join to the graph at the same vertex, and there is at least one line which is connected to one initial & one final state 4–momentum. Starting at one incoming momentum, the total energy s can only be fixed when one has reached the other initial state momentum in the graph, imposing a complicated constraint on the variables between p_a & p_b. Also intermediate state momenta may now be spacelike (see e.g. DIS) & some of the appropriate variables are now boosts.

The simplest possible recursion relation is based on the physical picture of sequential decay (see figure below):

$$R_n(p) = \int\int \frac{d^3\bar{p}_n}{2E_n} \prod_{i=1}^{n-1} \frac{d^3\bar{p}_i}{2E_i} \delta^4\left((p - p_n) - \sum_{i=1}^{n-1} p_i \right) = \int \frac{d^3\bar{p}_n}{2E_n} R_{n-1}(p - p_n)$$

R_{n-1} is only a function of $M_{n-1}^2 = (p - p_n)^2 = (p_1 + \ldots + p_{n-1})^2 \equiv k_{n-1}^2$

M_{n-1} is ofcourse the invariant mass of the system formed by particles 1, ..., n–1. Since R_{n-1} is a function of only 1 variable, it is most natural to take M_{n-1} as a variable of integration. When the following is inserted in integrand:

$$\int dM_{n-1}^2 \delta(M_{n-1}^2 - k_{n-1}^2) = 1, \int d^4k_{n-1} \delta^4(p - p_n - k_{n-1}) = 1 \quad \Rightarrow \quad R_n(M_n^2) =$$

$$\int dM_{n-1}^2 \int d^4k_{n-1} \int d^4p_n \delta(k_{n-1}^2 - M_{n-1}^2) \delta(p_n^2 - m_n^2) \delta^4(p - p_n - k_{n-1}) R_{n-1}(M_{n-1}^2)$$

(E.Byckling & K.Kajantie)

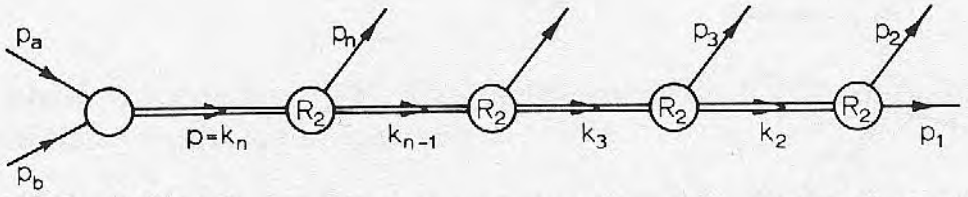

Figure VI.2.3 The reaction $p_a + p_b \to p_1 + \ldots + p_n$ expressed as a sequence of two-particle decays

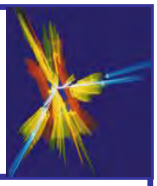

$$R_n(M_n^2) = \int_{\mu_{n-1}^2}^{(M_n - m_n)^2} dM_{n-1}^2 R_2(k_n; k_{n-1}^2, p_n^2) R_{n-1}(M_{n-1}^2)$$

$$= \int_{\mu_{n-1}^2}^{(M_n - m_n)^2} dM_{n-1}^2 \int d\Omega_{n-1} R_{n-1}(M_{n-1}^2) \sqrt{\lambda(M_n^2, M_{n-1}^2, m_n^2)} \Big/ 8M_n^2,$$

where $\mu_i = m_1 + \ldots + m_i$. Thresholds give $\mu_{n-1} \le M_{n-1} \le M_n - m_n$

So R_n can be expressed as a product of R_2 describing the decay $p \to p_n + k_{n-1}$ & R_{n-1} describing the decay $k_{n-1} \to p_1 + \ldots + p_{n-1}$, integrated over all possible values of the invariant mass M_{n-1}. To proceed, we iterate the above steps to obtain a relation corresponding to the entire chain. Let's use M_i instead of M_i^2 as variable. Then

$$R_n(M_n^2) = \frac{1}{2M_n} \int_{\mu_{n-1}}^{M_n - m_n} dM_{n-1} d\Omega_{n-1} \tfrac{1}{2} P_n \ldots \int_{\mu_2}^{M_3 - m_3} dM_2 d\Omega_2 \tfrac{1}{2} P_3 \int d\Omega_1 \tfrac{1}{2} P_2,$$

where $P_i = \sqrt{\lambda(M_i^2, M_{i-1}^2, m_i^2)} \Big/ 2M_i.$

The $3n-4$ essential variables now consists of 2 types:

(i) $n-2$ invariant masses M_i, $M_i^2 = k_i^2$, $i = 2, .., n-1$, defined the masses of the intermediate states.

(ii) $2(n-1)$ angles θ_i, ϕ_i in $\Omega_i = (\cos\theta_i, \phi_i)$, $i = 1, \ldots, n-1$. These define the direction of $\bar{k}_i = -\bar{p}_{i+1}$ in the rest frame $\bar{k}_{i+1} = 0$ of the decay $k_{i+1} \to p_{i+1} + k_i$ (see figure).

(E.Byckling & K.Kajantie)

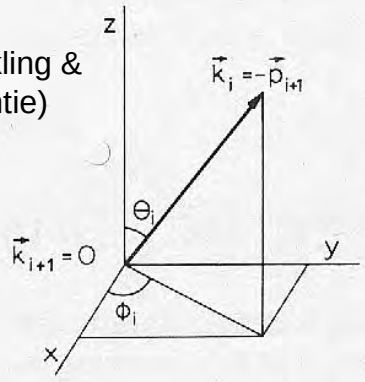

Figure VI.2.4 Definition of $\Omega_i = (\cos\theta_i, \phi_i)$. The orientation of coordinate axes can be chosen arbitrarily. To obtain the recursion relation (2.27) with multiperipheral momentum transfers, one chooses $\mathbf{p}_a$ as the z-axis and replaces $\cos\theta_i$ by the corresponding momentum transfer

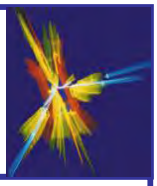

The equation can be used as basis for a generator. Let's examine 2 special cases: (i) all $m_i = 0$, equivalent with the asymptotic limit, M_n (or s) $\to \infty$ (the "ultrarelativistic" case):

$$R_n^{UR}(M_n^2) = R_n(s; m_i^2 = 0) = \left(\frac{\pi}{2}\right)^{n-1} \frac{s^{n-2}}{(n-1)!(n-2)!}$$

(ii) M_n (or s) $\to \mu_n = \Sigma m_i$ (the "non-relativistic" case):

$$R_n^{NR}(M_n^2) = R_n(s; m_i) = \frac{(2\pi^3)^{(n-1)/2}\sqrt{\prod_{i=1}^n m_i}}{2\Gamma\left\{\frac{3}{2}(n-1)\right\}\left(\sum_{i=1}^n m_i\right)^{3/2}}\left(\sqrt{s} - \sum_{i=1}^n m_i\right)^{(3n-5)/2}$$

A radically different relation for R_n is obtained by exploiting the freedom of choosing the variables of the intermediate R_i's in a tree diagram. If the direction of $\overline{p}_a$ is chosen as the z–axis, then the scattering angle, θ_{n-1}, of the process $p_a + p_b \to k_{n-1} + p_n$ can be replaced by the corresponding momentum transfer (see figure below).

$$t_{n-1} = (p_a - k_{n-1})^2 = m_a^2 + M_{n-1}^2 - 2E_a k_{n-1}^0 + 2P_a^{(n)} K_{n-1}\cos\theta_{n-1},$$

where $P_a^{(n)} = \sqrt{\lambda(M_n^2, m_a^2, m_b^2)}\big/2M_n$ & $K_{n-1} = \sqrt{\lambda(M_n^2, M_{n-1}^2, m_n^2)}\big/2M_n$

(E.Byckling & K.Kajantie)

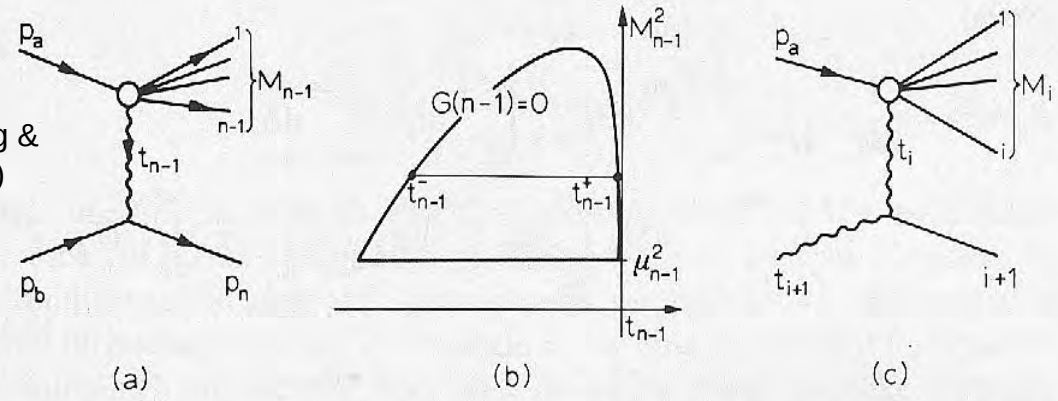

Figure VI.2.6 (a) The basic process when $\mathbf{p}_a$ is chosen as z axis in the frame $\mathbf{k}_n \equiv \mathbf{p}_a + \mathbf{p}_b = 0$; (b) the range of variation of t_{n-1} is given by the M_{n-1}^2, t_{n-1} Chew–Low plot; (c) the basic process at stage i of the iteration

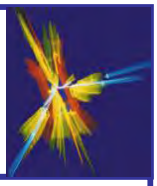

When $\cos\theta_{n-1}$ is replaced by t_{n-1}, the range $-1 \le \cos\theta_{n-1} \le 1$ is transformed to a M_{n-1}–dependent range $t_{n-1}^{-} \le t_{n-1} \le t_{n-1}^{+}$, where the specific values of $t_{n-1}^{\pm}$ are solutions to $G(n-1) \equiv G(s, t_{n-1}, m_n^2, m_a^2, m_b^2, M_{n-1}^2) = 0$. In terms of t_{n-1},

$$R_n(M_n^2) = \int_{\mu_{n-1}^2}^{(M_n - m_n)^2} dM_{n-1}^2 \int_{t_{n-1}^-}^{t_{n-1}^+} dt_{n-1} \int_0^{2\pi} d\phi_{n-1} \frac{R_{n-1}(M_{n-1}^2; t_{n-1})}{4\sqrt{\lambda(M_n^2, m_a^2, m_b^2)}},$$

where R_{n-1} has to be regarded as a function of t_{n-1}, since t_{n-1} is the (mass)^2 of one of the initial particles leading to R_{n-1}. To iterate, we must apply the same equation for R_{n-1} remembering that $m_b^2 \equiv t_n$ now has to be replaced by t_{n-1}. If we also take M_n as a variable instead of M_n^2, we obtain

$$R_n(M_n^2) = \frac{1}{2M_n} \cdot \frac{1}{4P_a^{(n)}} \int_{\mu_{n-1}}^{(M_n - m_n)} dM_{n-1} \int_{t_{n-1}^-}^{t_{n-1}^+} dt_{n-1} \int_0^{2\pi} d\phi_{n-1} \cdots \frac{1}{4P_a^{(3)}} \int_{\mu_2}^{(M_3 - m_3)} dM_2 \int_{t_2^-}^{t_2^+} dt_2 \int_0^{2\pi} d\phi_2 \times$$

$$\frac{1}{4P_a^{(2)}} \int_{t_1^-}^{t_1^+} dt_1 \int_0^{2\pi} d\phi_1, \text{ where } P_a^{(i)} = \sqrt{\lambda(M_i^2, t_i, m_a^2)} \Big/ 2M_i \ \ \& \ \ t_i = q_i^2, q_i = p_a - k_i$$

(E.Byckling & K.Kajantie)

In this equation, R_n can takes a form in which multiperipheral momentum transfers t_i appear as variables. That might be a more convient starting point for Monte Carlos than previous expression. One may also further replace the azimuthal angles ϕ_i in the above expression by invariants, which turns out to be equivalent to the 2–particle subinvariant masses s_i.

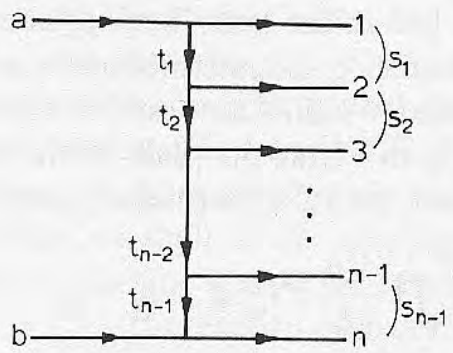

Figure VI.2.7 The multiperipheral momentum transfers $t_i = (p_a - p_1 - \ldots - p_i)^2$ and two-particle subenergies $s_i = (p_i + p_{i+1})^2$

DIS kinematics

Lepton-hadron scattering at sufficiently high energies create a large number of final state hadrons & such reactions are called **Deep Inelastic Scattering** (DIS). The reaction can generally be written as $a + N \rightarrow b + X$, where X stands for a hadronic system with an arbitrary number of particles, N a nucleon and a & b are leptons. As an example is electro-magnetic electron–proton DIS shown in the figure. The probe can either be electro-magnetic (γ), neutral (Z^0) or charged ($W^{\pm}$) current.

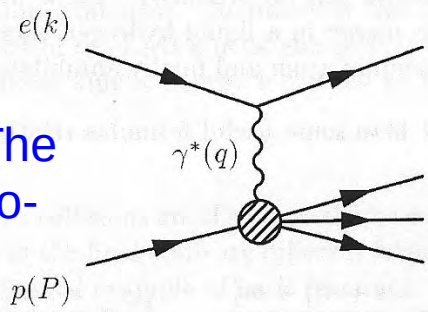

(von Schlippe)

Figure 2: Generic diagram of deep inelastic scattering.

To describe DIS reactions, we denote the 4–momentum of the incoming lepton by $k = (E,0,0,\boldsymbol{k})$, that of the target nucleon P and those of the scattered electron & hadronic system by k' and P', respectively. The exchanged boson has the 4–momentum $q = k - k'$. Convervation of the 4–momentum gives $k + P = k' + P'$. Since DIS–energies are at least a few GeV, the lepton masses can safely be set = 0. Then the 4–momentum transfer squared $q^2 = (k-k')^2 \approx -2EE'(1-cos\theta) \leq 0$, i.e. the exchanged boson is spacelike.

The invariant $W^2 = P'^2$ is DIS–variable since the hadronic system can have variable multiplicity. The kinematics of a DIS reaction is therefore determined by 3 independent invariants rather than 2 as in the case in $2 \rightarrow 2$ scattering. The reaction is called ”deep” since $-q^2 \gg m_N^2$ & inelastic since final state X not just a nucleon (& usually $W^2 \gg m_N^2$).

DIS kinematics

A natural choice of one of these invariants is $S = (k + P)^2 = m_N^2 + 2k \cdot P$, which is defined the experimental setup. The 2nd invariant is usually chosen to be the negative (4–momentum transfer)^2, $Q^2 = -q^2 = 4EE'\cos^2(\theta/2)$. The 3rd independent invariant can be taken to be W or one of the dimensionless variables $x = Q^2/(2P \cdot q)$ *or* $y = (P \cdot q)/(k \cdot P)$. The invariant x is called Bjorken–x and gives the fraction of the nucleon momentum carried by the involved parton. The variable y has a simple physical meaning in TF: $y = 1 - E^{T\prime}/E^T$ i.e. the relative energy loss of the lepton.

In fixed target DIS, $S = m_N^2 + 2m_N E_a$, whereas in a lepton–proton collider like HERA $S = 4E_a E_p$. Note following useful DIS variable relations $Q^2 \approx xyS$ & $W^2 \approx m_N^2 + Q^2(1/x - 1)$. Within the parton model framework, the process can be viewed as below with the lepton–quark collision as the **hard subprocess**. If we think of the incoming lepton and nucleon as travelling in opposite directions, then at sufficiently high momenta, the energy of the quark is the same fraction of the nucleon energy i.e. x. Then the subprocess invariant $s = (k + p)^2 = xS$, where p (= xP) is the 4–momentum of the incoming quark.

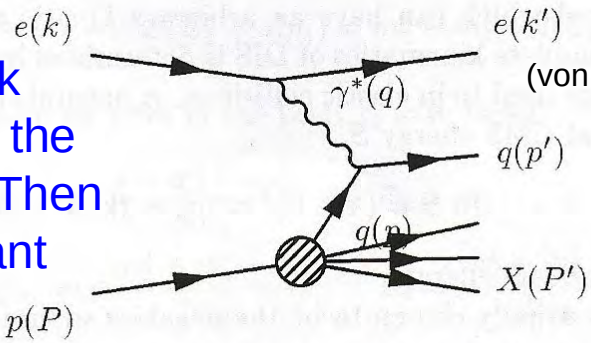

(von Schlippe)

Figure 3: Parton model diagram of deep inelastic scattering.

One is naturally interested in the parton content of the proton (to be able to describe e.g. proton–proton processes).

Parton distribution functions

The proton content is described by the parton distribution functions (**pdf's**) that gives the momentum distribution in the proton separately for each partons species (e.g. for a (anti)quark flavour or gluons). The kinematics of the parton process is controlled by 2 variables, x & Q^2 so then also the proton pdf's $f_i(x, Q^2)$ are functions of both x & Q^2. Below is shown the underlying physics reasons for the experimentally observed shape of the valence quark pdf.

(F.Halzen & A.Martin)

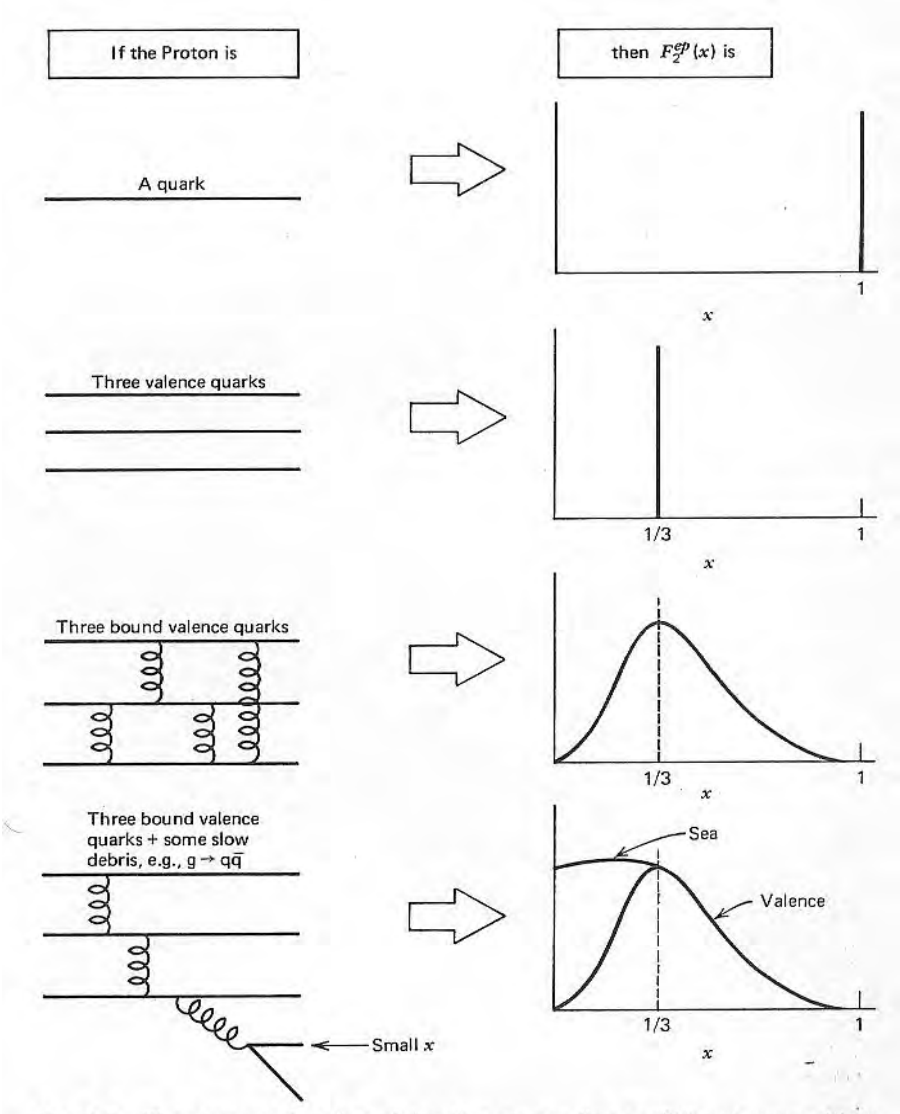

Fig. 9.7 The structure function pictured corresponding to different compositions assumed for the proton.

Structure functions

The cross section for neutral–current & charged–current reactions can be written in terms of 3 structure functions:

$$\frac{d^2\sigma^{ii}}{dxdy} = \frac{4\pi\alpha^2}{xyQ^2}\eta_{ii}\left\{\left(1-y-\frac{m_N^2x^2y^2}{Q^2}\right)F_2^{ii} + y^2xF_1^{ii} \pm \left(y-\frac{y^2}{2}\right)xF_3^{ii}\right\}$$

where $ii = \gamma, \gamma Z, Z$ corresponds to neutral–current, $l(\nu) + N \rightarrow l(\nu) + X$, processes & $ii = W$ to charged–current, $l(\nu) + N \rightarrow \nu(l) + X$, processes. The structure functions, F_j^{ii}, are functions of x & Q^2. In the last term, the + & – sign is for reactions with incoming lepton & antilepton, respectively. The factor η_{ii} is the ratio of the corresponding propagator & coupling to the photon propagator & coupling.

$$\eta_\gamma = 1; \eta_{\gamma Z} = \left(\frac{G_F m_Z^2}{2\pi\alpha\sqrt{2}}\frac{Q^2}{Q^2+m_Z^2}\right); \eta_Z = \eta_{\gamma Z}^2; \eta_W = \tfrac{1}{2}\left(\frac{G_F m_W^2}{4\pi\alpha}\frac{Q^2}{Q^2+m_W^2}\right)^2$$

In the parton model interpretation, the structure functions $F_j^{ii}(x, Q^2)$ can be expressed in terms of the quark pdf's.

$$F_2^\gamma = x\sum_q e_q^2(q+\bar{q}); F_2^{\gamma Z} = x\sum_q 2e_q v_q(q+\bar{q}); F_2^Z = x\sum_q (v_q^2+a_q^2)(q+\bar{q})$$

$$F_3^\gamma = 0; F_3^{\gamma Z} = \sum_q 2e_q a_q(q-\bar{q}); F_3^Z = \sum_q 2v_q a_q(q-\bar{q}); 2xF_1^{ii} = F_2^{ii},$$

where e_q is the electric charge, v_q (= $\pm$½ – $2e_q \sin^2\theta_W$) the vector coupling & a_q (= $\pm$½) the axial vector coupling of quark q. The $F_j^{W-}(x, Q^2)$–pdf relations are the following:

$$F_2^{W-} = 2x(u+\bar{d}+\bar{s}+c...); F_3^{W-} = 2(u-\bar{d}-\bar{s}+c...); 2xF_1^{W-} = F_2^{W-},$$

where only active flavours are to be included. The F_j^{W+}'s obtained by interchanges $d \leftrightarrow u$ & $s \leftrightarrow c$ in F_j^{W-}-formula.

The parton model predicts that the structure functions F_i^{ii} converge at fixed x when $Q^2 \to \infty$ however this is violated because of hard gluon radiation. This scale-dependence is predicted in perturbative QCD via "DGLAP"-equations:

$$\frac{\partial(q_i - \bar{q}_i)}{\partial \ln \mu^2} = \frac{\alpha_s(\mu^2)}{2\pi} \int_x^1 \frac{dz}{z} P_{qq}(z)(q_i(x/z, Q^2) - \bar{q}_i(x/z, Q^2))$$

$$\frac{\partial}{\partial \ln \mu^2} \begin{pmatrix} (q_i + \bar{q}_i) \\ g \end{pmatrix} = \frac{\alpha_s(\mu^2)}{2\pi} \begin{pmatrix} P_{qq} & 2N_F P_{qg} \\ P_{qg} & P_{gg} \end{pmatrix} \otimes \begin{pmatrix} (q_i + \bar{q}_i) \\ g \end{pmatrix}$$

where $P_{ij}(z)$ gives the probability for a $i \to j$ splitting with momentum fraction z. Note that even if QCD can predict the evolution of pdf's from a particular scale, μ_0, it cannot predict them at any μ without having experimental measurements as inputs.

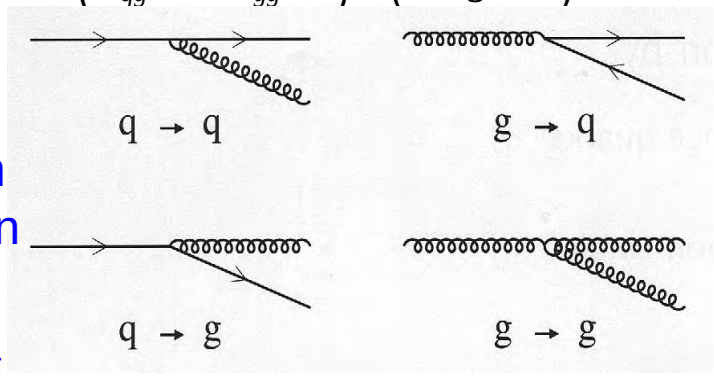

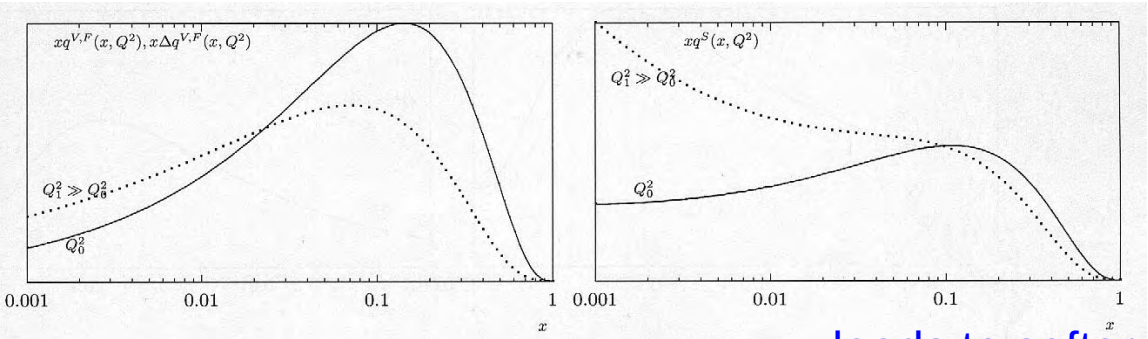

Qualitative effects of DGLAP:

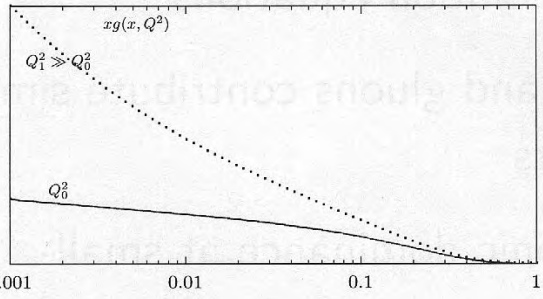

leads to softer pdf's & larger number of partons. large–x: valence quarks dominate, small–x: gluons.

Determination of pdfs

The pdfs determined using an iterative procedure based on a functional ansatz combined with DGLAP evolution & experimental data. Several determinations exist: notably CTEQ & MRST. Both use a very wide data, x & Q^2 range.

Process	Main Subprocess	PDFs Probed
$\ell^{\pm}N \to \ell^{\pm}X$	$\gamma^* q \to q$	$g(x \lesssim 0.01), q, \bar{q}$
$\ell^+(\ell^-)N \to \overline{\nu}(\nu)X$	$W^* q \to q'$	
$\nu(\overline{\nu})N \to \ell^-(\ell^+)X$	$W^* q \to q'$	
$\nu N \to \mu^+\mu^- X$	$W^* s \to c \to \mu^+$	s
$pp \to \gamma X$	$qg \to \gamma q$	$g(x \sim 0.4)$
$pN \to \mu^+\mu^- X$	$q\bar{q} \to \gamma^*$	$\bar{q}$
$pp, pn \to \mu^+\mu^- X$	$u\bar{u}, d\bar{d} \to \gamma^*$	$\bar{u} - \bar{d}$
	$u\bar{d}, d\bar{u} \to \gamma^*$	
$ep, en \to e\pi X$	$\gamma^* q \to q$	
$p\bar{p} \to W \to \ell^{\pm}X$	$ud \to W$	$u, d, u/d$
$p\bar{p} \to$ jet $+X$	$gg, qg, qq \to 2j$	$q, g(0.01 \lesssim x \lesssim 0.5)$

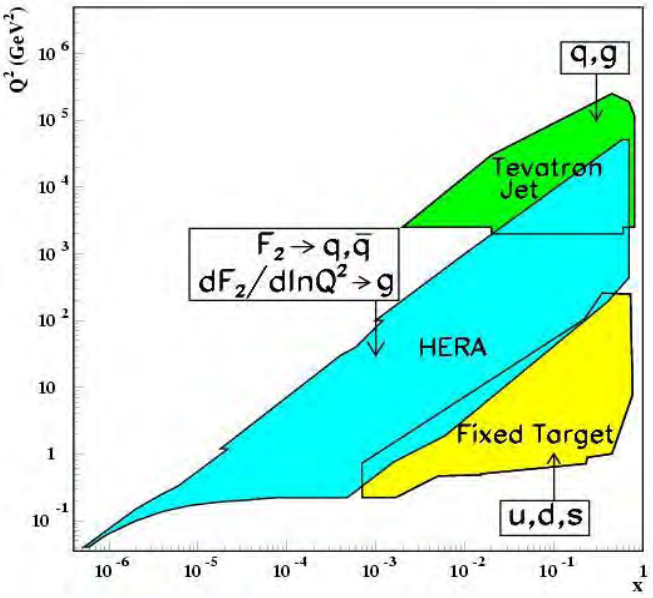

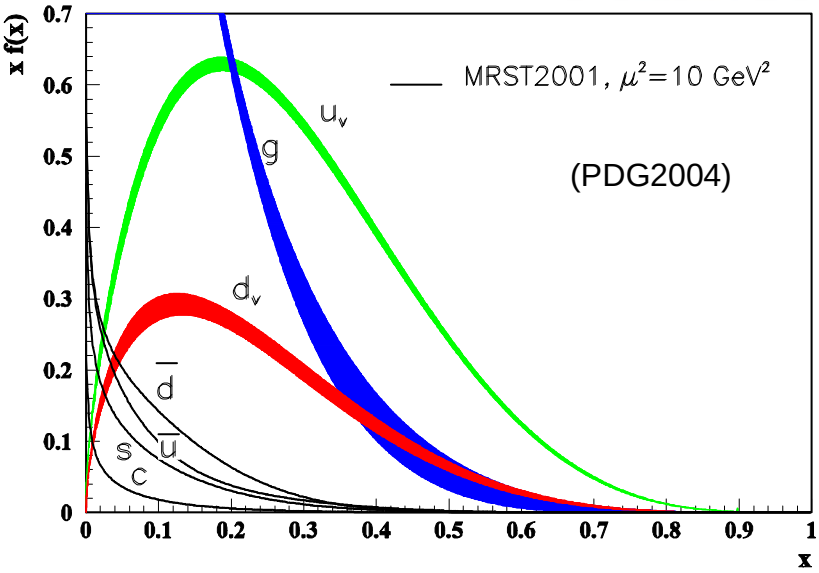

The output are pdf's for different flavours at some x & Q^2 as the distribution here to your left.

In hadron–hadron collisions, usually pdf's are one of the largest uncertainties in measurements of cross sections, etc … (at best known they are known to 5-10 % but in certain corners of the Q–x plane the uncertainty can be much larger).

Electron positron annihilation

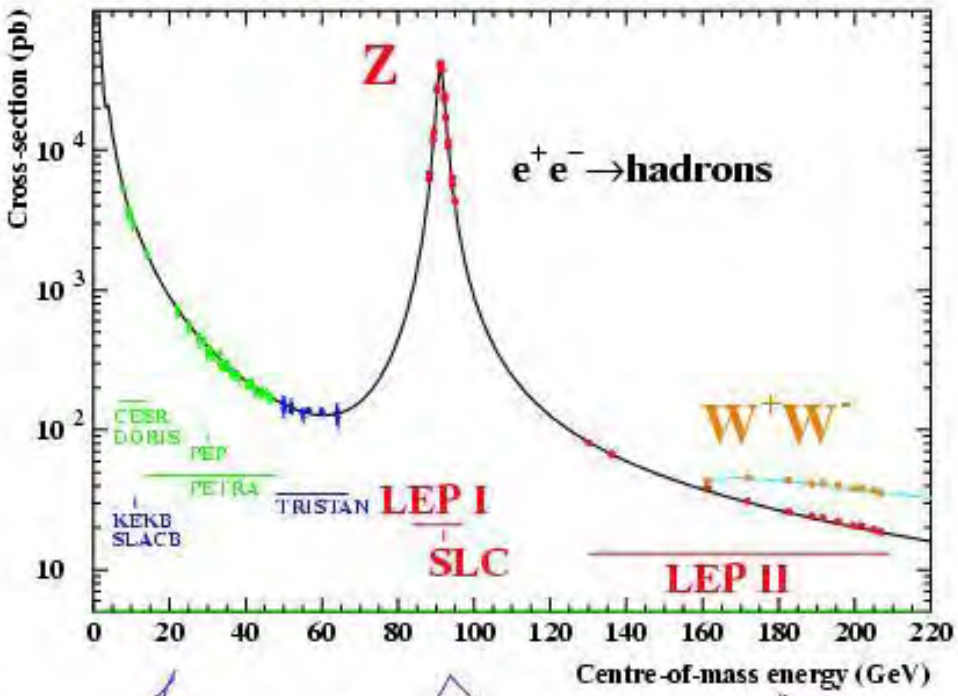

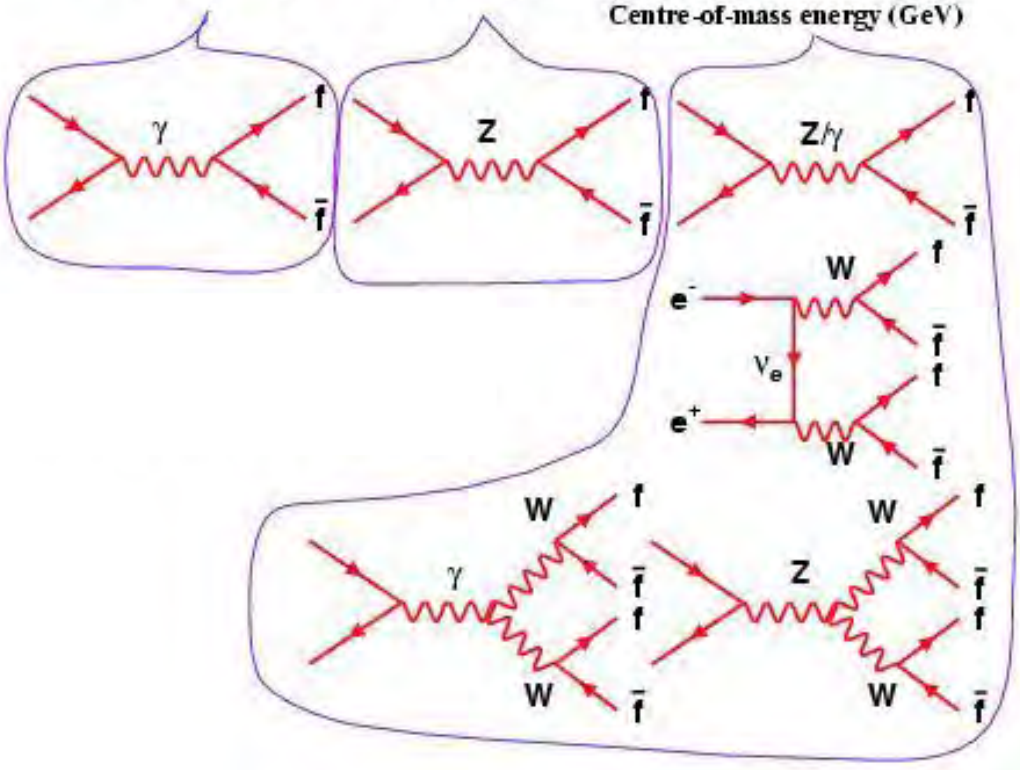

e^+e^- cross sections

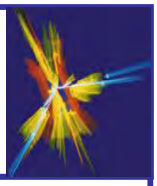

For pointlike spin-½ fermions, the CMF differential cross section for $e^+e^- \to f\bar{f}$ via single γ exchange (N_C = 1 (leptons) or 3 (quarks), θ = angle between incoming e^- & produced f) is:

$$\frac{d\sigma}{d\Omega}(e^+e^- \to f\bar{f}) = N_C \frac{\alpha^2}{4s} Q_f^2 \beta\left[1+\cos^2\theta + (1-\beta^2)\sin^2\theta\right],$$

where β is the velocity of the final state fermion in CMF and Q_f is the charge of the fermion. For $\beta \to 1$, $\sigma = 4\pi\alpha^2 N_C Q_f^2 / 3s$. At higher energies, the Z^0 must be included. If the mass of a fermion f is much less than the mass of the Z^0, then the differential cross section for $e^+e^- \to f\bar{f}$ is

$$\frac{d\sigma}{d\Omega}(e^+e^- \to Z^0/\gamma \to f\bar{f}) = N_C \frac{\alpha^2}{4s}\{(1+\cos^2\theta)[Q_f^2 - 8\chi_1 v_e v_f Q_f + 16\chi_2(a_e^2+v_e^2)(a_f^2+v_f^2)] + 2\cos\theta[-8\chi_1 a_e a_f Q_f + 64\chi_2 a_e a_f v_e v_f]\},$$

where $\chi_{1[2]} = \frac{1}{16[^2](\sin^2\theta_W \cos^2\theta_W)^{1[2]}} \frac{s(s-M_Z^2)[s/(s-M_Z^2)]}{(s-M_Z^2)^2 + M_Z^2\Gamma_Z^2}$, $a_f = T_{3L}^f$,

$v_f = T_{3L}^f - 2Q_f \sin^2\theta_W$; $T_{3L}^f = \frac{1}{2}(-\frac{1}{2})$ for up(down) - type q's & ν (charged l's)

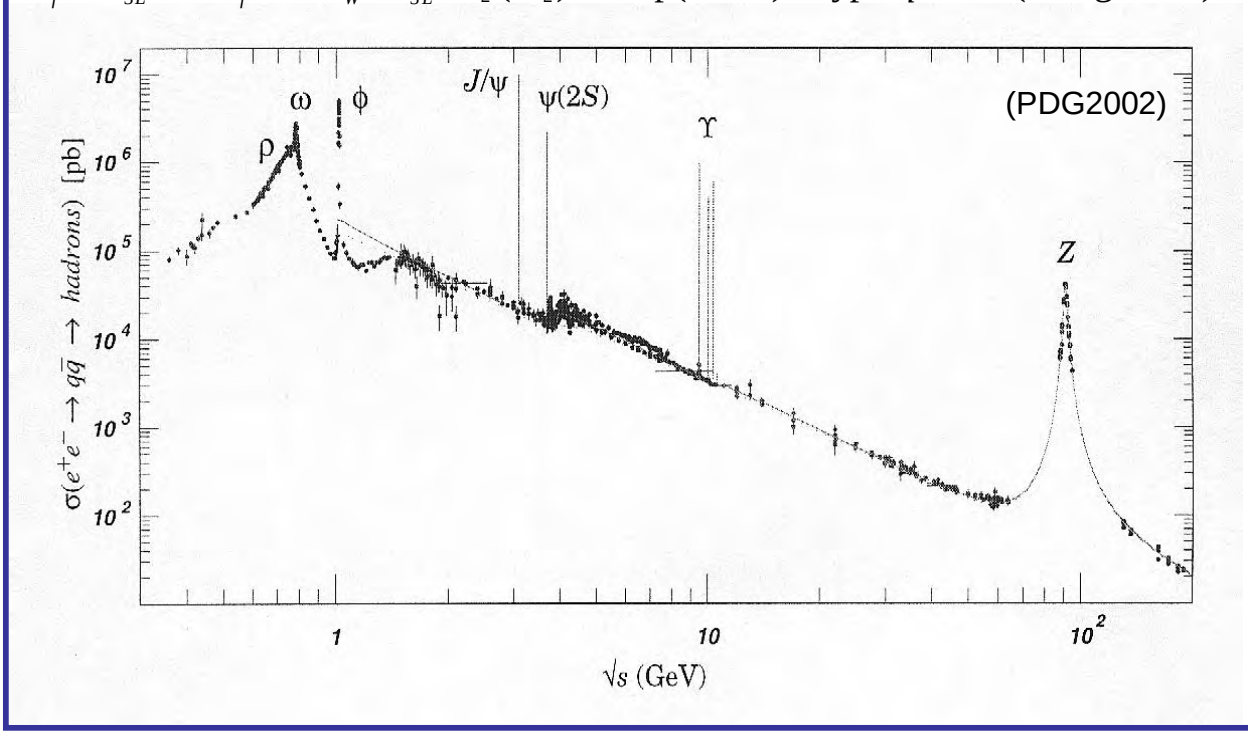

Parton fragmentation functions

The parton fragmentation function $D_i^h(x, Q^2)$ describes the probability to produce a certain hadron h from the parton i (= q, $\bar{q}$ ... g) & are analogous to the pdf's obtain from DIS.

In the fragmentation function x represents the fraction of the partons momentum carried by a produced hadron h, whereas in the pdf, it represents the fraction of a original hadrons momentum carried by the constituent parton. Q^2 describes the energy scale at parton production (= $\sqrt{s}$) instead of the momentum transfer as for the pdf's in DIS.

The fragmentation functions $D_i^h(x, Q^2)$ exhibit similar scaling violations as the pdf's $f_i(x, Q^2)$ from DIS and their Q^2 evolution is described by similar "DGLAP"–equations:

$$\frac{\partial D_i(x,Q^2)}{\partial \ln Q^2} = \sum_j \int_x^1 \frac{dz}{z} \frac{\alpha_s}{2\pi} P_{ji}(z,\alpha_s) D_j(x/z, Q^2),$$

$$\text{where} \quad P_{ji}(z,\alpha_s) = P_{ji}^{(0)}(z,\alpha_s) + \frac{\alpha_s}{2\pi} P_{ji}^{(1)}(z,\alpha_s) + \ldots$$

The lowest–order functions $P_{ji}^{(0)}(z)$ are the same as those for the pdf's of DIS but higher–order terms are different. Note that the splitting function now is P_{ji} rather than P_{ij}, since D_j describes the fragmentation of the final parton. So P_{ji} is the probability for parton i to transfer into parton j.

The effect of the Q^2 evolution is the same as for DIS pdf's: x–distribution shifted towards lower values for larger Q^2's. The P_{ji}'s contain singularities at z = 0 & z =1, which have important effects on fragmentation at small & large x, for details see O. Biebel, P. Nason & B.R. Webber, hep-ph/0109282.

Parton fragmentation functions

The parton fragmentation function $D_i^h(x,s)$ are usually determined from the e^+e^- fragmentation functions $F^h(x,s)$.

$$F^h(x,s) = \frac{1}{\sigma_{\text{tot}}}\frac{d\sigma}{dx}(e^+e^- \to hX) = \sum_i \int_x^1 \frac{dz}{z} C_i(s;z,\alpha_s) D_i^h(x/z,s),$$

where $C_q(s;z,\alpha_s) = g_q(s)\delta(1-z) + O(\alpha_s)$ & $C_g(s;z,\alpha_s) = O(\alpha_s)$

and $g_i(s)$ is the appropriate (e.g. q) electroweak coupling.

The e^+e^- fragmentation functions for all charged particles for different $\sqrt{s}$. The influence of scaling violations can be seen. Larger $\sqrt{s}$ shifts the x–distribution towards smaller x's.

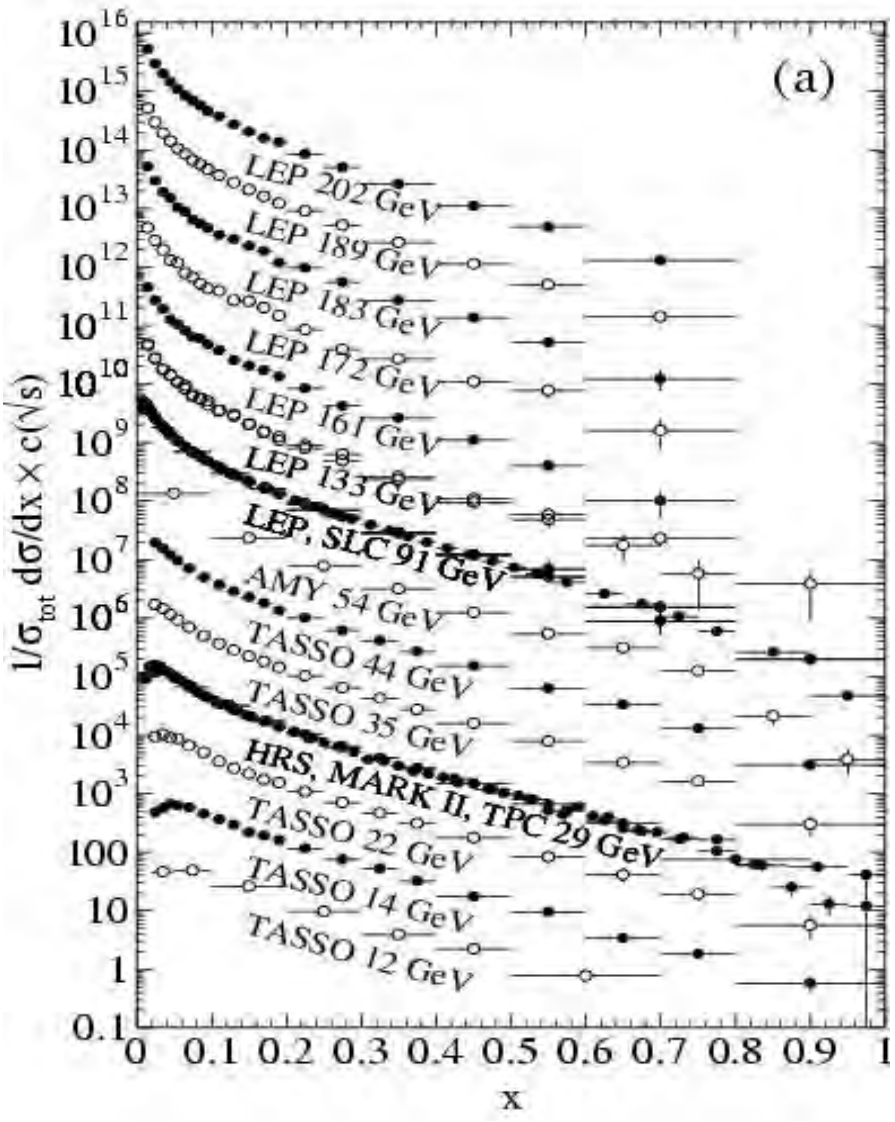

Parton fragmentation functions

In $e^+e^- \to \gamma/Z^0 \to hX$, the differential distribution w.r.t. to x & the angle θ between the hadron h and the incoming e^+:

$$\frac{1}{\sigma_{\text{tot}}}\frac{d^2\sigma}{dx\,d\cos\theta}(e^+e^- \to hX) = \frac{3}{8}(1+\cos^2\theta)\,F_T(x,s) + \frac{3}{4}\sin^2\theta\,F_L(x,s),$$

where $F_L(x,s)$ & $F_T(x,s)$ are the longitudinal & transverse fragmentation functions that represents the contributions from virtual bosons that are longitudinally or transversely polarized w.r.t. to the direction of the motion of the hadron.

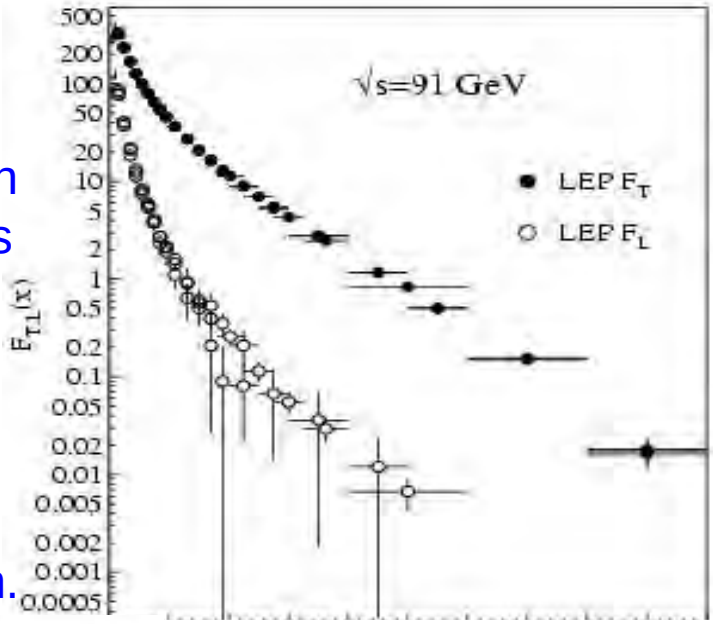

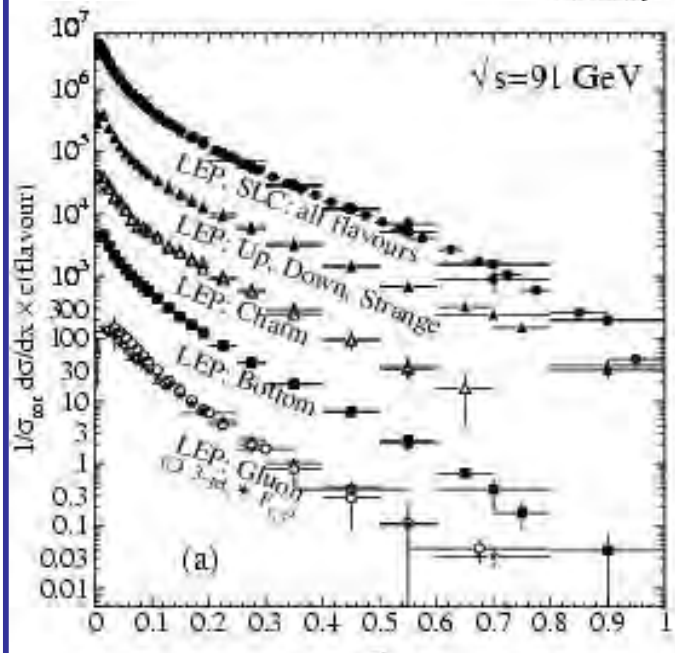

The gluon fragmentation function $D_g(x)$ can be extracted from the measured $F_T(x)$ & $F_L(x)$ since the coefficient functions C_i's of q & g are related at order $O(\alpha_s)$.

$$F_L(x,s) = C_F\frac{\alpha_s}{2\pi}\int_x^1 \frac{dz}{z}\left[F_T(z,s) + 4\left(\frac{z}{x}-1\right)D_g(z,s)\right] + O(\alpha_s^2) \quad \& C_F = \frac{4}{3}$$

Fragmentation of heavy quarks

The fragmentation of heavy quarks (c & b) is a separate case since the heavy flavoured hadron will retain a large fraction of the momentum of the original quark, in the limit of infinitely heavy quarks, the fragmentation function becomes $\delta(1-x)$. Considerably larger than when light quarks fragment.

If the heavy quark is produced at momenta much larger than its mass, large perturbative effects are expected.

The inclusion of non-perturbative effects is in practice done by convoluting the perturbative result with some phenomenological model. Below some popular ones:

$$\text{Peterson et al.:} \quad D_Q(x) \propto \frac{1}{x}\left(1-\frac{1}{x}-\frac{\varepsilon}{1-x}\right)^{-2}$$

$$\text{Kartvelishvili et al.:} \quad D_Q(x) \propto x^{\alpha}(1-x)$$

$$\text{Lund}-\text{description:} \quad D_Q(x) \propto \frac{1}{x}x^{\alpha}\left(\frac{1-x}{x}\right)^{\alpha}\exp\left(-\frac{\beta m_Q^2}{x}\right),$$

where ε, α & β are quark dependent parameters parametrizing the non–perturbative effects. On the left the experimental measurement of the fragmentation function for b–quarks.

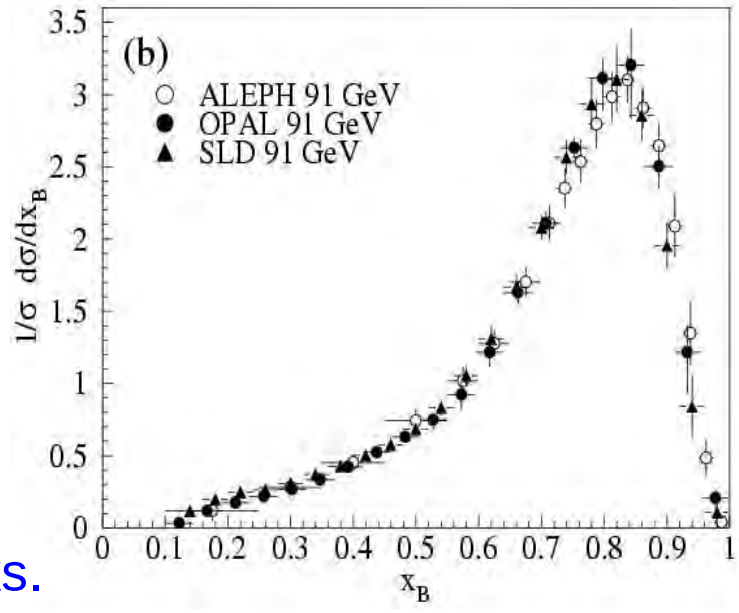

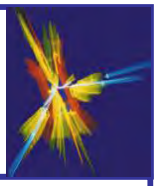

Hadron-hadron interactions

protons complex objects: partonic substructure: quarks & gluons

hard scattering processes (large momentum transfer):

(R.Field)

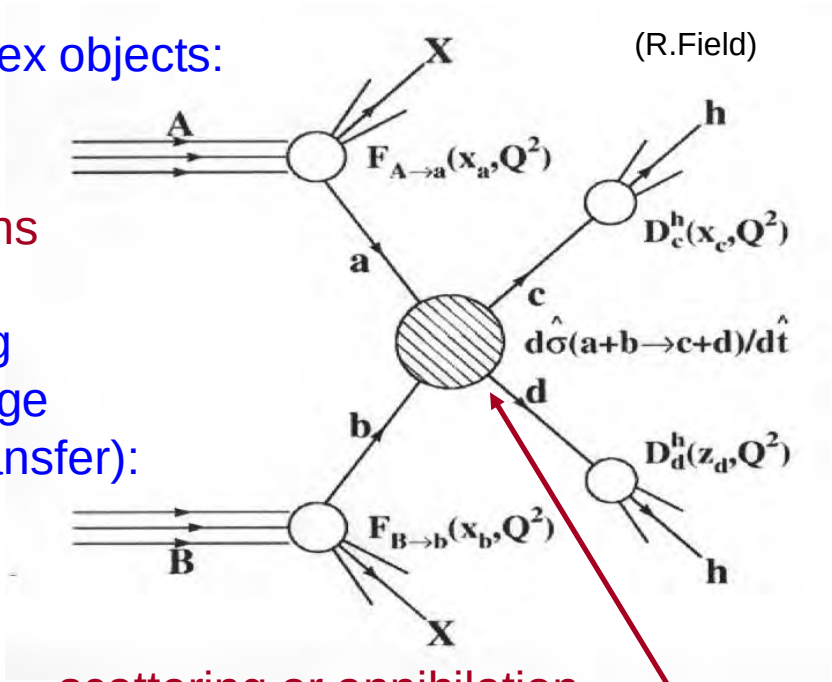

quark-quark
quark-gluon scattering or annihilation
gluon-gluon

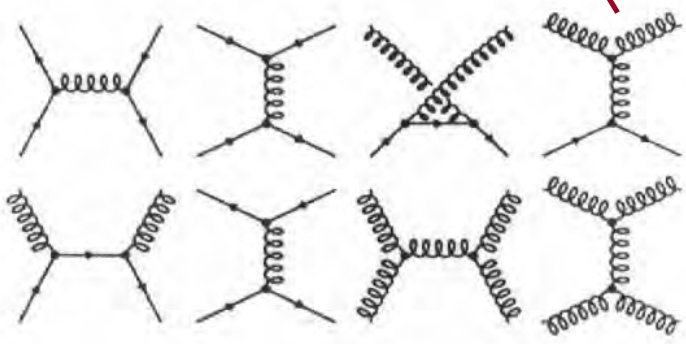

at parton level

However: hard scattering (i.e. high p_T processes) represent only a tiny fraction of the total inelastic pp cross section.

e.g. total inelastic cross section ~80 mb at $\sqrt{s}$ = 14 TeV.

Dominanted by events with small momentum transfer of which there are essentially two types: minimum-bias (color exchange) & diffractive events (no exchange of quantum numbers).

Inelastic low p_T hadron-hadron collisions

Most interactions due to interactions at large distance between incoming protons where protons interact as "a whole" → small momentum transfer ($\Delta p \approx \hbar / \Delta x$) → particles in final state have large longitudinal momentum but small transverse momentum.

$< p_T > \approx 0.5$ GeV (of charged particles in final state)

These are called minimum-bias events ("soft" events). They are a large fraction of the total cross section e.g. ~60 mb at $\sqrt{s}$ = 14 TeV. They are perhaps not very interesting in themselves but needs to be understood. Cross section so huge that they overlap normal collisions ("pile-up") & change measured quantities.

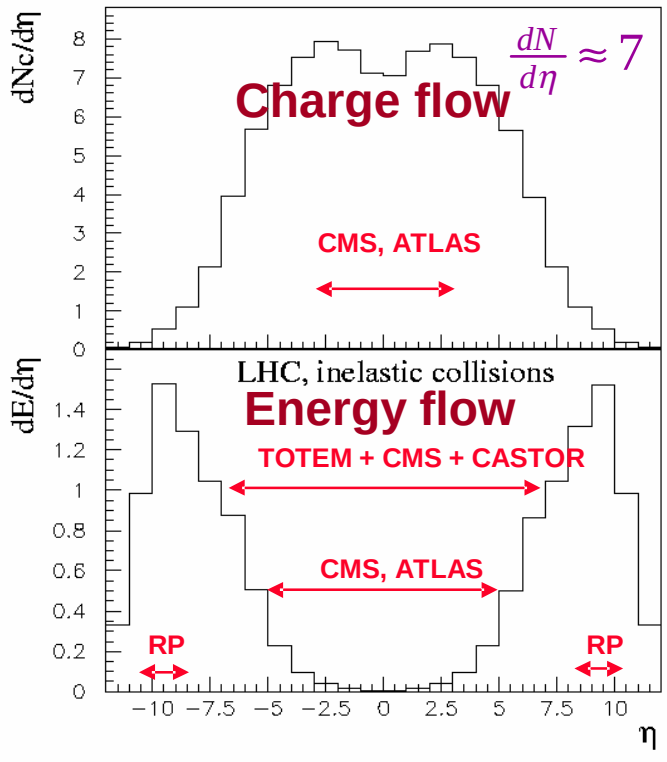

The charged particle & the energy flow in an average LHC proton-proton collision. The acceptancies of the baseline ATLAS & CMS experiments are also indicated.

Diffractive processes

Another large part of the total cross section are diffractive processes, where non-colored objects are exchanged
(often refered to as "Pomerons", nowadays described by gluon systems)

Diffractive events characterized by "rapidity gaps" (void of particles)

elastic scattering ~30 mb, single diffraction ~14 mb & double diffraction ~7 mb; in total ~50 mb at $\sqrt{s}$ = 14 TeV.

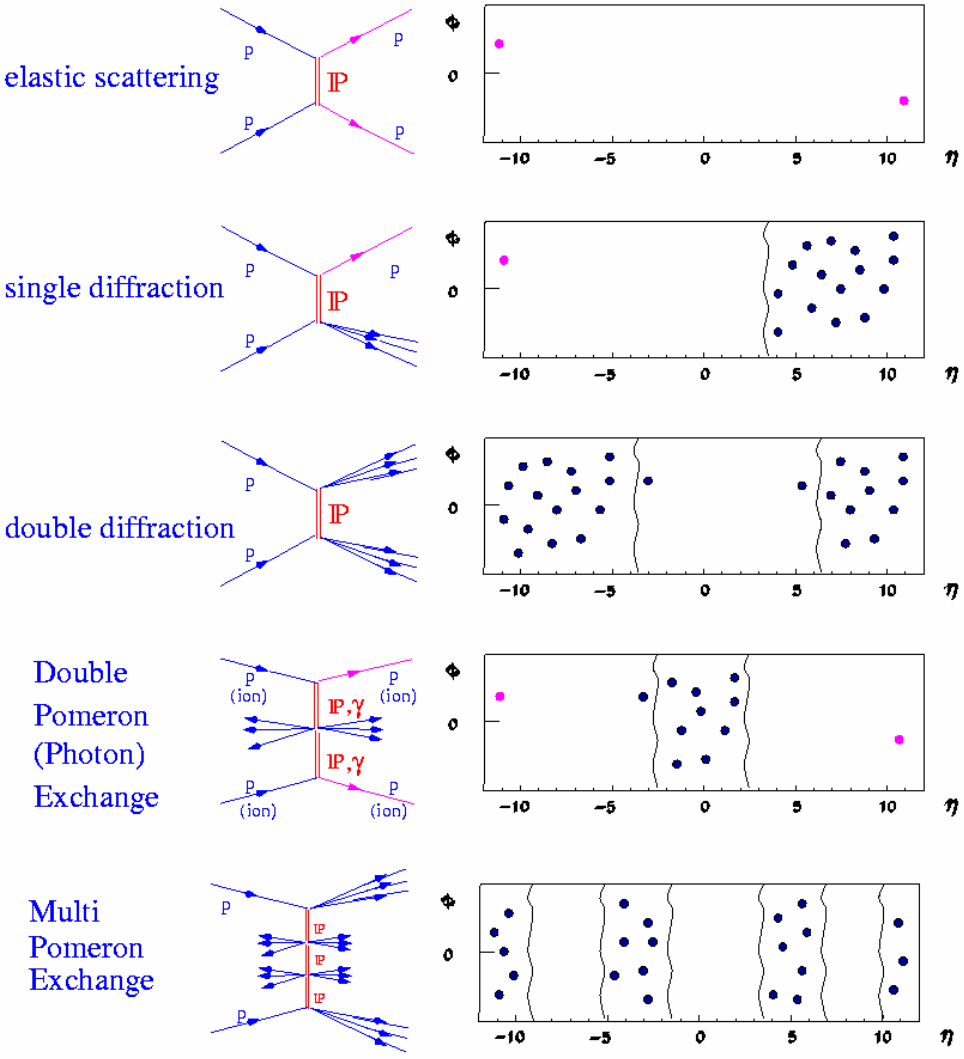

Inelastic high p_T hadron-hadron collisions

Proton beam can be seen as a beam of quarks & gluons with a wide band of energies. Occasionally occurs hard scattering between constituents of incoming hadrons.

Constituents carry a fraction $0 < x < 1$ of the proton momentum.

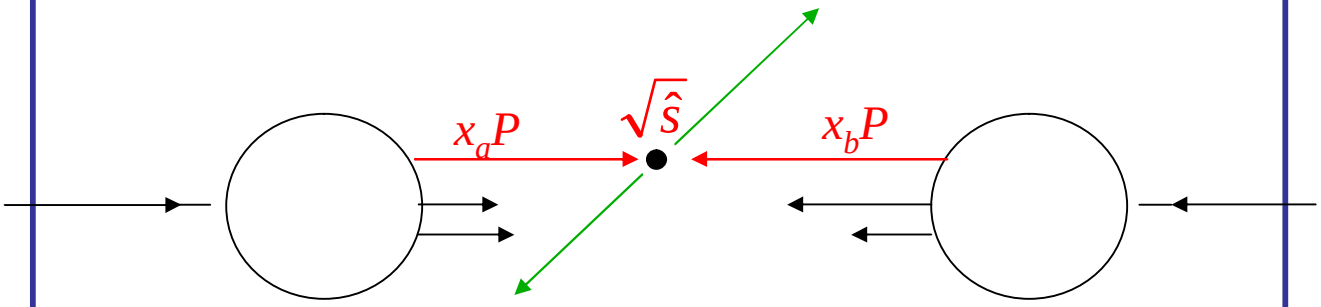

$P \equiv$ momentum of incoming hadron

The effective center-of-mass energy $\sqrt{\hat{s}}$ usually much smaller than $\sqrt{s}$.

$$\bar{p}_a = x_a \bar{p}_A$$
$$\bar{p}_b = x_b \bar{p}_B$$

if $x_a \approx x_b$

$$\sqrt{\hat{s}} = \sqrt{x_a x_b s} \approx x\sqrt{s}$$

to produce a mass of:

	LHC	Tevatron
100 GeV:	$x \sim 0.007$	$x \sim 0.05$
1 TeV:	$x \sim 0.07$	$x \sim 0.5$

These are interesting physics events but they are rare.

e.g. $\bar{u} + d \rightarrow W^-$

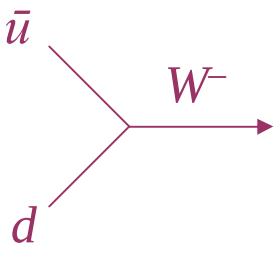

$$\sigma(pp \rightarrow W) \approx 150 \text{ nb} \approx \mathbf{10^{-6}}\, \sigma_{\text{tot}}(pp)$$

Hadron-hadron interactions

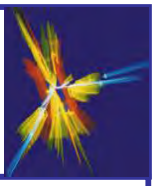

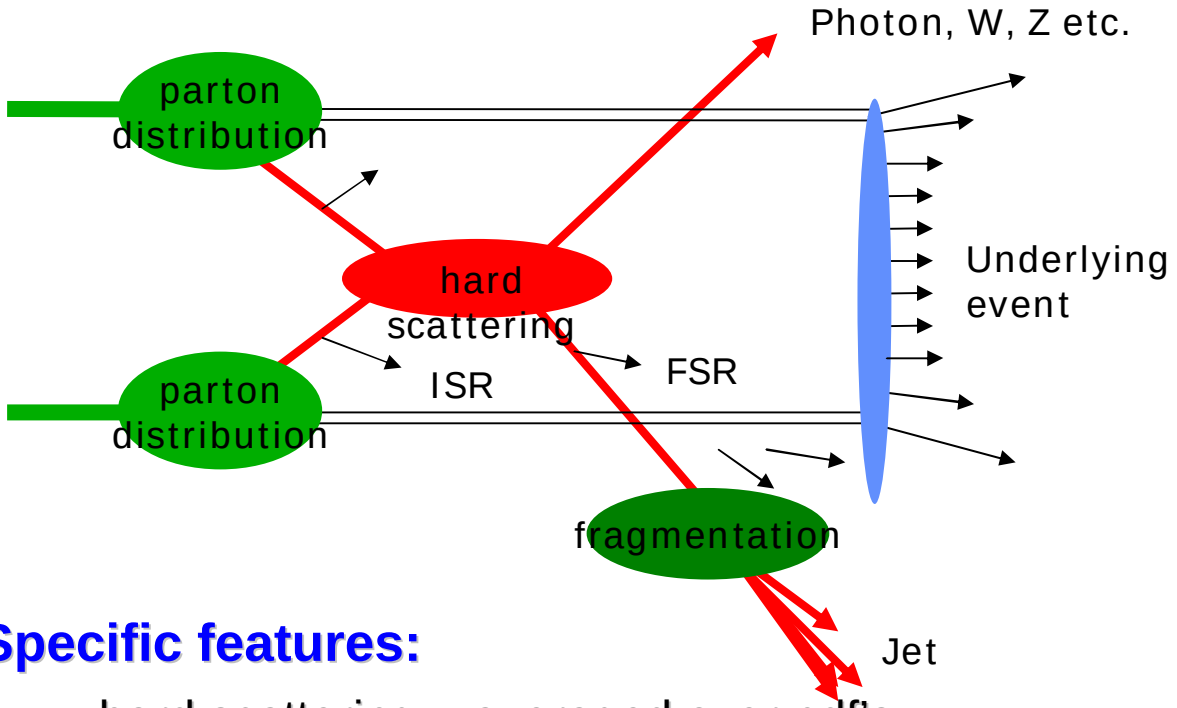

Specific features:

- hard scattering σ averaged over pdf's
- initial and final states can emit gluons
- colored final states fragment to form "jets"
- underlying event from proton/antiproton remnants

Fragmentation (hadronization):

- quarks & gluons produce lots of radiation (α_S is large!) & recombine to form colorless spray of almost collinear hadrons: a jet.
- jets are the experimental signature of quarks or gluons and is seen as localized calorimeter energy deposits.
- jet energy ≠ parton energy due to missing particles (e.g. ν's, low p_T & out of cone particles), overlapping particles (from underlying event or other jets) & especially the calorimeter response. Corrections based on averages applied to the measured jet energy.

At hadron colliders jets usually formed using simple cone algorithms ($R \approx 0.4$)

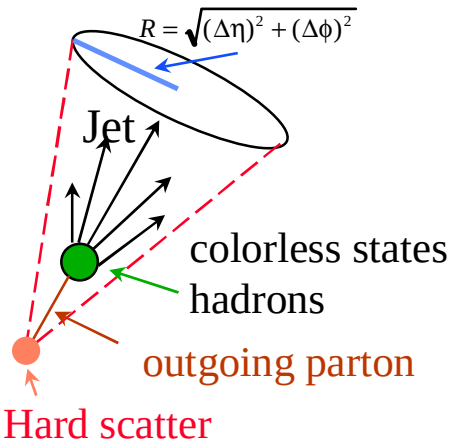

- cross-section :

$$\sigma = \sum_{a,b} \int dx_a\, dx_b\; f_a(x_a, Q^2)\, f_b(x_b, Q^2)\, \hat{\sigma}_{ab}(x_a, x_b)$$

$\hat{\sigma}_{ab}$ ≡ hard scattering cross-section

$f_i(x, Q^2)$ ≡ parton distribution function

parton distribution functions measured in DIS & hadron-hadron collisions

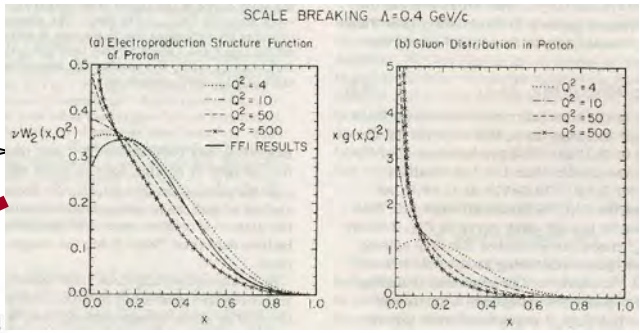

(R.Field)

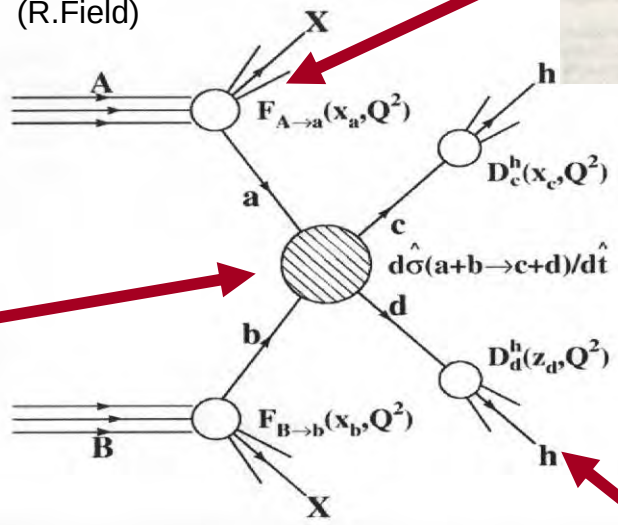

quark & gluon fragmentation functions measured mostly in e^+e^- collisions; modeled by fragmentation MC

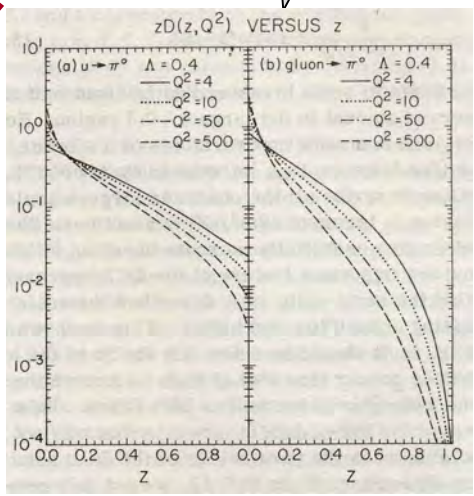

TABLE I. Cross sections for the various constituent quark-quark, quark-gluon, and gluon-gluon subprocesses.[3] The differential cross section is given by $d\hat{\sigma}/d\hat{t} = \pi\alpha_s^2(Q^2)|A|^2/\hat{s}^2$, where $\alpha_s(Q^2)$ is the effective coupling given by Eq. (3.1).

	Subprocess	$\lvert A\rvert^2$
1.	$q_i q_j \to q_i q_j$ $q_i \bar{q}_j \to q_i \bar{q}_j$ $(i \neq j)$	$\frac{4}{9}\frac{\hat{s}^2+\hat{u}^2}{\hat{t}^2}$
2.	$q_i q_i \to q_i q_i$	$\frac{4}{9}\left(\frac{\hat{s}^2+\hat{u}^2}{\hat{t}^2}+\frac{\hat{s}^2+\hat{t}^2}{\hat{u}^2}\right)-\frac{8}{27}\frac{\hat{s}^2}{\hat{u}\hat{t}}$
3.	$q_i \bar{q}_i \to q_i \bar{q}_i$	$\frac{4}{9}\left(\frac{\hat{s}^2+\hat{u}^2}{\hat{t}^2}+\frac{\hat{t}^2+\hat{u}^2}{\hat{s}^2}\right)-\frac{8}{27}\frac{\hat{u}^2}{\hat{s}\hat{t}}$
4.	$q_i \bar{q}_i \to gg$	$\frac{32}{27}\left(\frac{\hat{u}^2+\hat{t}^2}{\hat{u}\hat{t}}\right)-\frac{8}{3}\left(\frac{\hat{u}^2+\hat{t}^2}{\hat{s}^2}\right)$
5.	$gg \to q_i \bar{q}_i$	$\frac{1}{6}\left(\frac{\hat{u}^2+\hat{t}^2}{\hat{u}\hat{t}}\right)-\frac{3}{8}\left(\frac{\hat{u}^2+\hat{t}^2}{\hat{s}^2}\right)$
6.	$q_i g \to q_i g$	$-\frac{4}{9}\left(\frac{\hat{u}^2+\hat{s}^2}{\hat{u}\hat{s}}\right)+\left(\frac{\hat{u}^2+\hat{s}^2}{\hat{t}^2}\right)$
7.	$gg \to gg$	$\frac{9}{2}\left(3-\frac{\hat{u}\hat{t}}{\hat{s}^2}-\frac{\hat{u}\hat{s}}{\hat{t}^2}-\frac{\hat{s}\hat{t}}{\hat{u}^2}\right)$

quark & gluon cross-sections calculable in QCD